Electronic Supplementary Information for:

Office Paper and Laser Printing: A Versatile and Affordable Approach for Fabricating Paper-Based Analytical Devices with Multimodal Detection Capabilities

Lucas R. Sousa[a,b], Barbara G. S. Guinati[a], Lanaia I. L. Maciel[a], Thaisa A. Baldo[a], Lucas C. Duarte[a], Regina M. Takeuchi[c], Ronaldo C. Faria[d], Boniek G. Vaz [a], Thiago R. L. C. Paixão[e,f] and Wendell K. T. Coltro[a,e]*

[a]*Instituto de Química, Universidade Federal de Goiás, 74690-900, Goiânia, GO, Brazil*

[b]*Laboratorio de Biosensores y Bioanálisis (LABB), Departamento de Química Biológica e IQUIBICEN´ − CONICET, Facultad de Ciencias Exactas y Naturales, Universidad de Buenos Aires (UBA), Pabell ó n 2, Ciudad Universitaria, Ciudad Autónoma de Buenos Aires, Argentina*

[c]*Instituto de Ciências Exatas e Naturais do Pontal, Universidade Federal de Uberlândia, 38304-402, Ituiutaba, MG, Brazil*

[d]*Departamento de Química, Universidade Federal de São Carlos,* 13565-905*, São Carlos, SP, Brazil*

[e]*Instituto Nacional de Ciência e Tecnologia de Bioanalítica, 13084-971, Campinas, SP, Brazil*

[f]*Departamento de Química Fundamental, Instituto de Química, Universidade de São Paulo, 05508-900, São Paulo, SP, Brazil*

***Corresponding Author:**

Professor Wendell K. T. Coltro

Instituto de Química, Universidade Federal de Goiás

Campus Samambaia, 74690-900

Goiânia, GO, Brazil

Fax: +55 62 3521 1127

E-mail: wendell@ufg.br

ORCID: http://orcid.org/0000-0002-4009-2291

Experimental

PhotoMetrix as a colorimetric tool

Colorimetric measurements were made using a smartphone model iPhone XR equipped with a 12MP resolution camera (Apple Inc., California, EUA) equipped with the PhotoMetrix® application were used to capture and analyze the digital images. The app is available for free download at the Apple Store, and in the literature, reports and protocol protocols are available for the use of this app for colorimetric analysis in paper-based analytical devices[1,2].

The images were captured under ambient light conditions, and the capture distance was standardized using a 5 cm photo capture support. The region of interest (ROI) was selected considering the microzones' diameter, and the pixel´s average was evaluated in the area previously defined (32 x 32 pixels).

The RGB model quantifies color intensity in a three-dimensional space, and other models like HSV, HSL, and HSI can be derived from it. Value, lightness, and intensity represent the amount of light in a color. After image acquisition, various processing techniques can be applied in the Photometrix® application to enhance image features. The application captures image data and converts it into RGB histograms, allowing for color-intensity analysis. It is noteworthy that usually color intensity is reported as arbitrary units. This is due to the fact that the measurement depends on instrument settings and experimental conditions (e.g. use of different smartphone cameras or background light). The term “arb. units” (or a.u.), when used to represent the y-axis, provides qualitative guidance.

Instrumental parameters of PSI-MS

Mass spectra were recorded using a Thermo Scientific LTQ XL Linear Ion trap mass spectrometer (San Jose, USA). To monitor methyldopa we used the intensity of protonated ions. The spectra were collected for 1 min, and the extracted ion chromatogram intensities were used to monitor the analyte. The instrumental parameters were as follows: positive ionization mode, spray voltage at 4 kV, capillary temperature 275 °C, capillary voltage at 40 V, tube lens at 40 V and collision energy for MS/MS analyses 25 manufacturer’s unit (mu). The spectra were processed using the Xcalibur Analysis software package (version 2.0, Service Release 2, Thermo Electron Corporation).

Results

Formation of toner barriers on office paper substrates

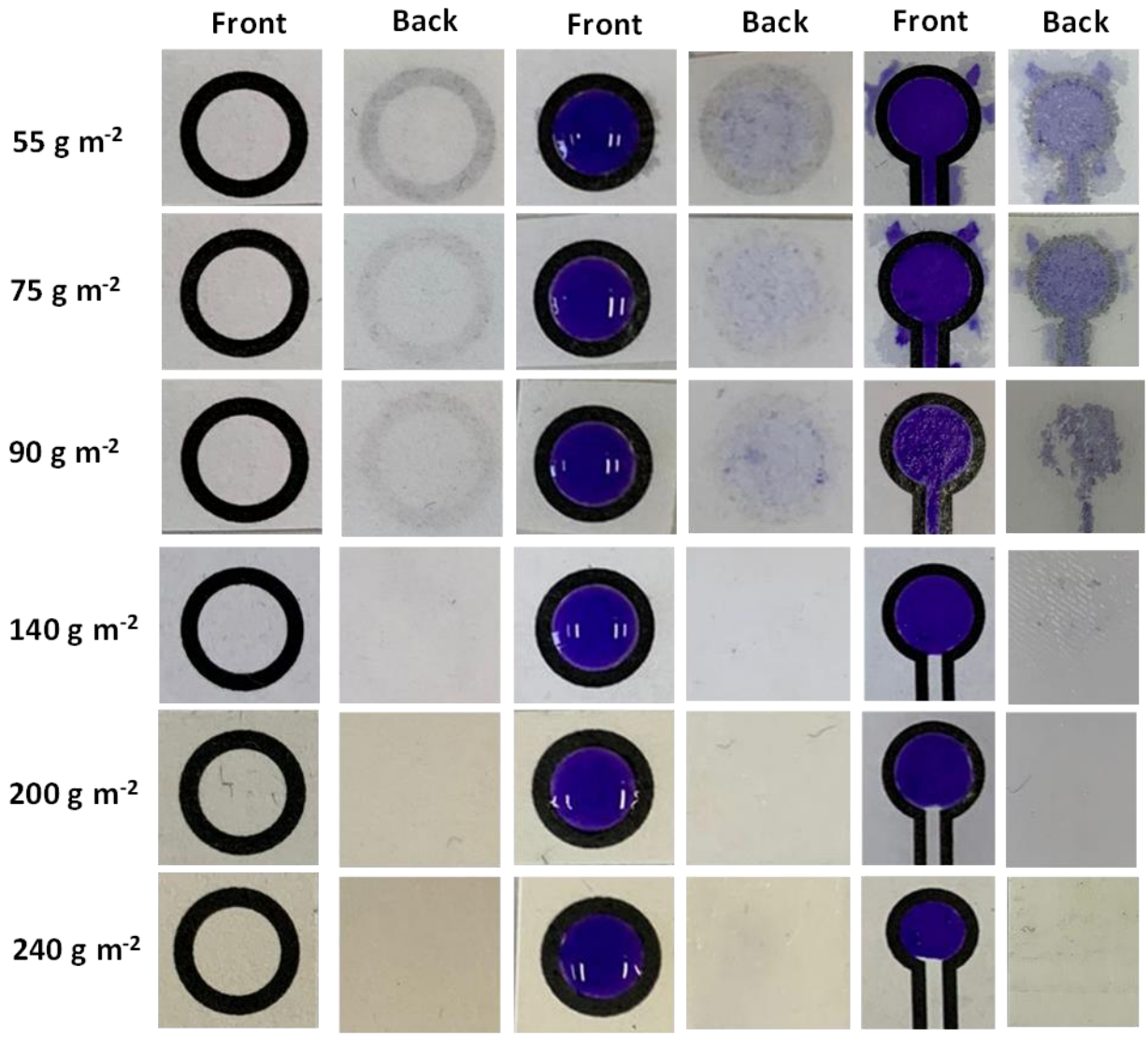

Figure S1. Optical images showing the front and back sides of microzones and µPADs manufactured using laser printing technique on different grammages of office paper.

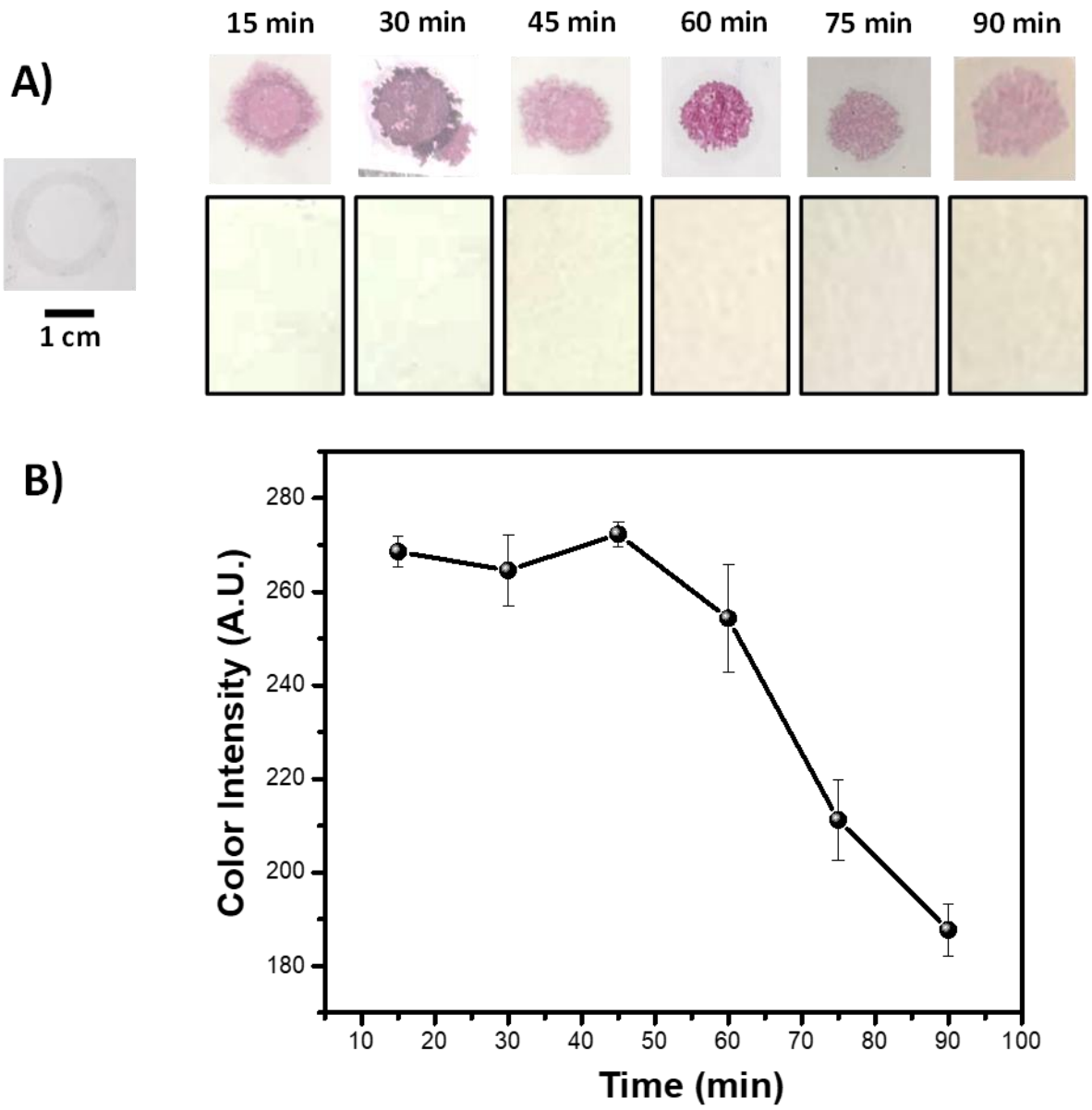

Figure S2. Comparison of the efficiency of barrier formation at different time intervals when heated at 200 ºC. In (A) optical images showing the back side of microzones (A) and comparison of paper coloration at these time intervals (B).

Colorimetric reaction for Par detection

A colorimetric method based on a redox reaction described previously was optimized for Par determination using office paper devices. For this, an iron chloride (III) and potassium hexacyanoferrate (III) solutions were used as chromogenic reagents[3]. The reaction is based on reduction of Fe(III) into Fe(II), which is chelated to $K_3[Fe(CN)_6$ forming Prussian blue, which is a blue colored product as shown in the reactions bellow:

$$Par + Fe^{3+} \rightarrow Fe^{2+} + \text{oxidized product}$$

$$Fe^{2+} + K_3[Fe(CN)_6] \rightarrow KFe[Fe(CN)_6] + 2K^+$$

The intensity and time of the blue color formed is dependent on Par concentration, in this way, the chromogenic reagents concentration was evaluated, and optimal concentration was established in 1.23 mmol L^{-1} for iron chloride (III) and 10 mmol L^{-1} for potassium hexacyanoferrate (III), which provided the higher color intensity. The optimal pH to perform the reaction is between 5.0 – 6.0. In these conditions the colorimetric reaction occurs in 5 minutes.

Griess reaction for Nitrite and Nitrate colorimetric detection

The nitrite and nitrate were monitored using the Griess method based on sulfanilamide (50 mmol L^{-1}), N-(1-naphthyl) ethylenediamine (4 mmol L^{-1}) and nitrite reaction, forming a red-pink azo dye. The Griess method does not show a response for nitrate, however, nitrate can be reduced to nitrite by a zinc powder suspension, and then the Griess reaction can proceed. The paper surface was oxidized with 0.5 mol L^{-1} sodium periodate and washed three times with distilled water. The reduction should be performed in neutral conditions to prevent zinc oxidation. The colorimetric reaction was performed in acid conditions using citric acid (160 mmol L^{-1}). In these conditions the colorimetric reaction occurs in 10 minutes.

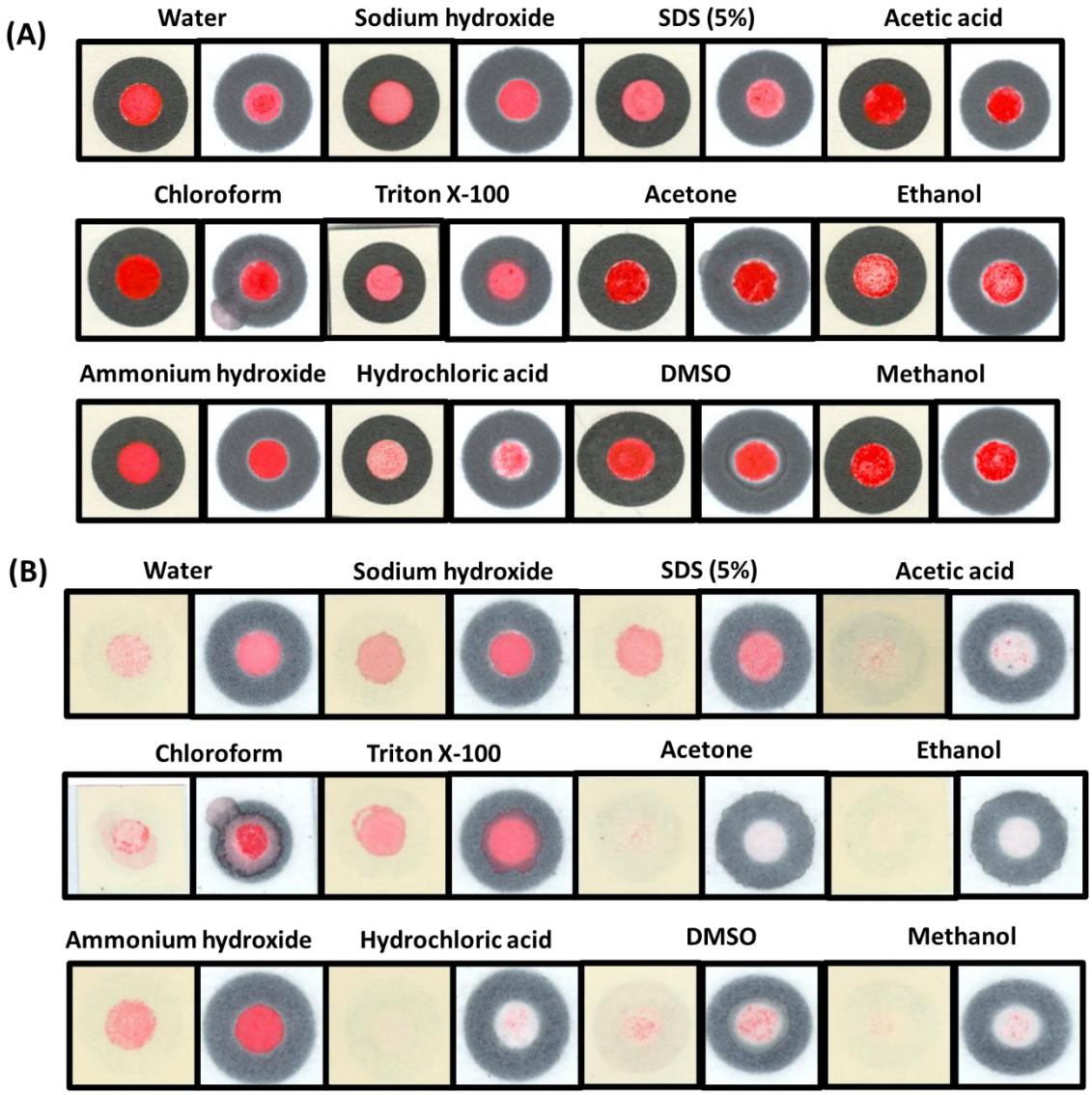

Figure S3. Optical images showing the **(A)** front side and **(B)** back side of microzones to evaluate the chemical resistance of barriers defined with toner laser printing (left side) in comparison to wax barriers (right side) when exposed to different surfactants (5% SDS and triton X-100), organic solvents (chloroform, acetone, ethanol, methanol, and DMSO) and acids (1 mol L^{-1} acetic acid and 0.1 mol L^{-1} hydrochloric acid) and bases (1 mol L^{-1} ammonium hydroxide and 0.1 mol L^{-1} sodium hydroxide).

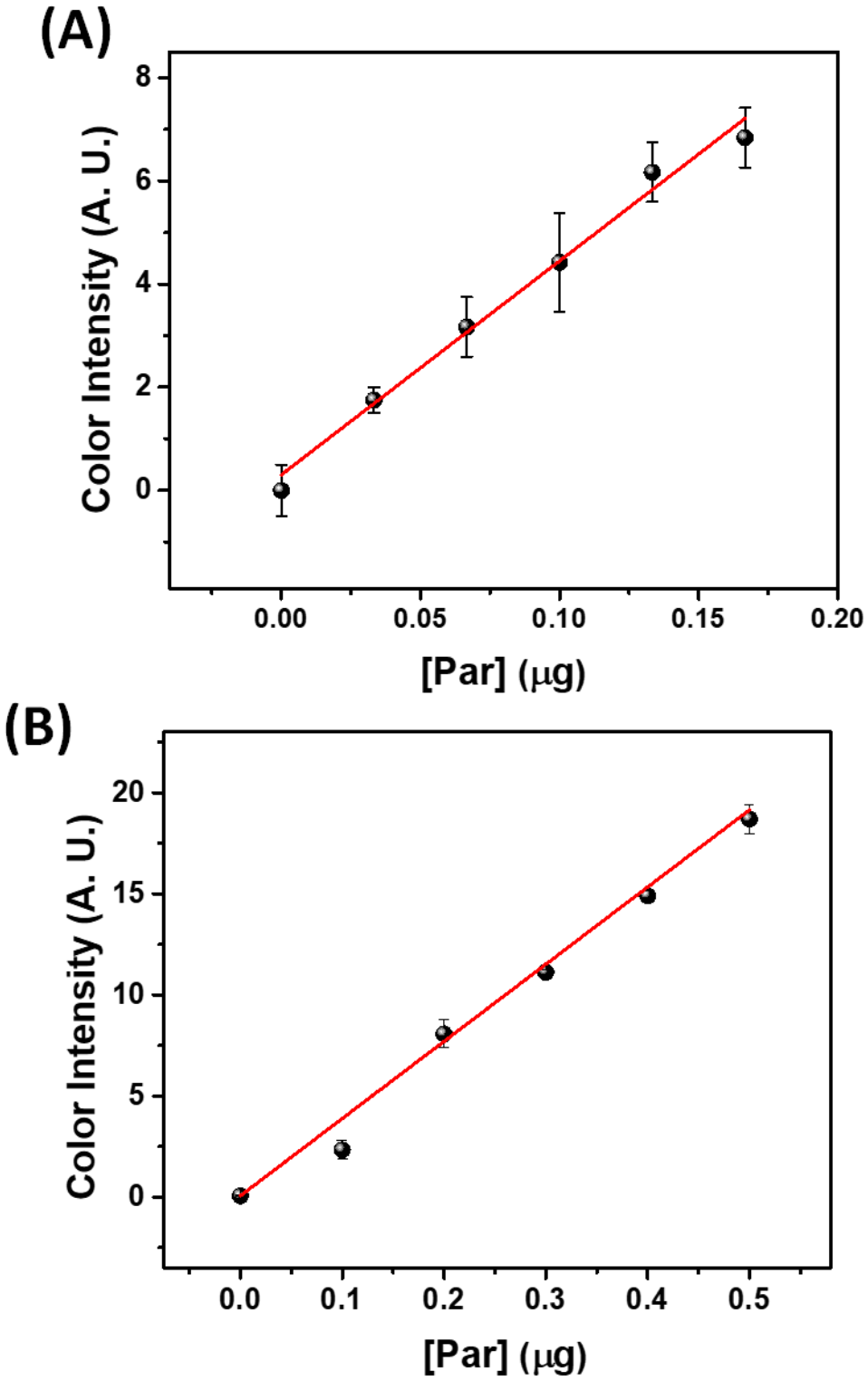

Figure S4: Optical images and analytical curves for Par assay using **(A)** office paper and **(B)** chromatographic paper devices. The linear regression equations were: $y_{color\ intensity}$ = 0.30 + 41.43×[Par] (r^2 = 0.995) for office paper device, and y = 0.07 + 38.17×[Par] (r^2 = 0.998) for chromatographic paper device. Each symbol (●) represents the average of colour intensity for triplicate measurements and the error bars indicate the standard deviations.

Table S5. Comparison of the estimated limit of detection for the analytes with those reported in the literature.

Analyte	Detection method	Detection range	LOD	Ref.
Par	Electrochemical	0.05 – 2.0 mmol L^{-1}	10 µmol L^{-1}	[4]
Par	Electrochemical	50 – 350 µmol L^{-1}	15 µmol L^{-1}	[5]
Par	Electrochemical	0.1 – 1.0 mmol L^{-1}	0.046 mmol L^{-1}	[6]
Par	Colorimetric	0.075 – 0.18 µg	0.04 µg	This work
Iron	Colorimetric	1.5 – 15µg	0.75 µg	[7]
Iron	Colorimetric	1.0 – 20 mg L^{-1}	0.1 mg L^{-1}	[8]
Iron	Distance-colorimetric	20 -100 ppm	not specified	[9]
Iron	Distance-colorimetric	20 – 100 mg mL^{-1}	4.5 mg mL^{-1}	This work
Nitrite	Colorimetric	5 – 55 µmol L^{-1}	0.09 µmol L^{-1}	[10]
Nitrite	Colorimetric	1 – 250 mg kg^{-1}	1.1 mg kg^{-1}	[11]
Nitrite	Colorimetric	5 – 250 µM	0.05 µM	[12]
Nitrite	Colorimetric	20 – 100 µmol L^{-1}	6.8 µmol L^{-1}	This work
Nitrate	Colorimetric	0.01 - 50 mg L^{-1}	0.53 mg L^{-1}	[13]
Nitrate	Colorimetric	0.2 – 1.2 mM	0.08 mM	[12]
Nitrate	Colorimetric	20 – 100 µmol L^{-1}	2.7 µmol L^{-1}	This work
PSA	Colorimetric	0.5 – 45.0 ng·mL^{-1}	0.4 ng mL^{-1}	[14]
PSA	Electrochemistry	10 - 0.05 µg L^{-1}	0.05µg L^{-1*}	[15]
PSA	Electrochemistry	60 - 0.09 µg L^{-1}	0.09 µM L^{-1}	[16]
PSA	Electrochemical	$1x10^{-5}$ – 100 ng mL^{-1}	0.048 fg mL^{-1}	This work

*Limit of quantitation

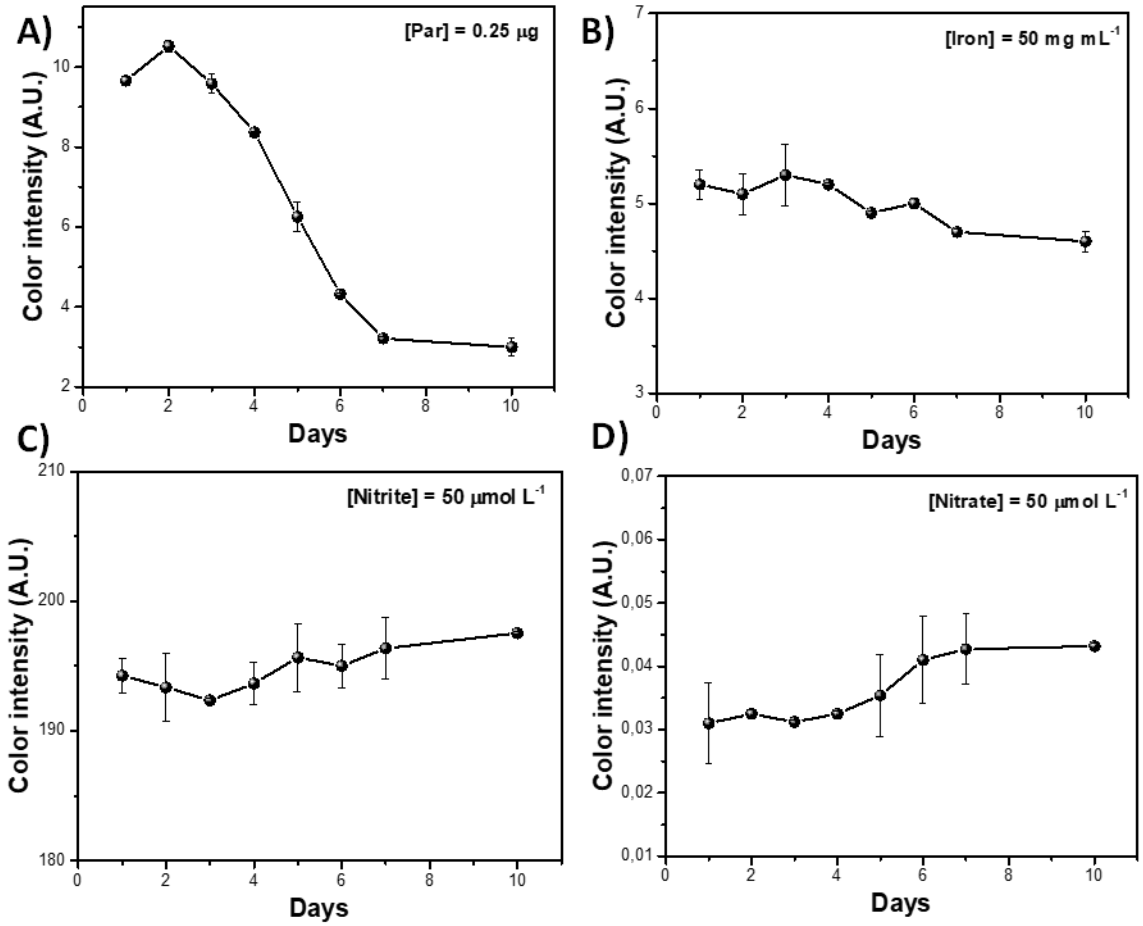

Figure S6. Durability study of office paper devices for colorimetric analysis of Par (A), Iron (B), Nitrite (C) and Nitrate (D)

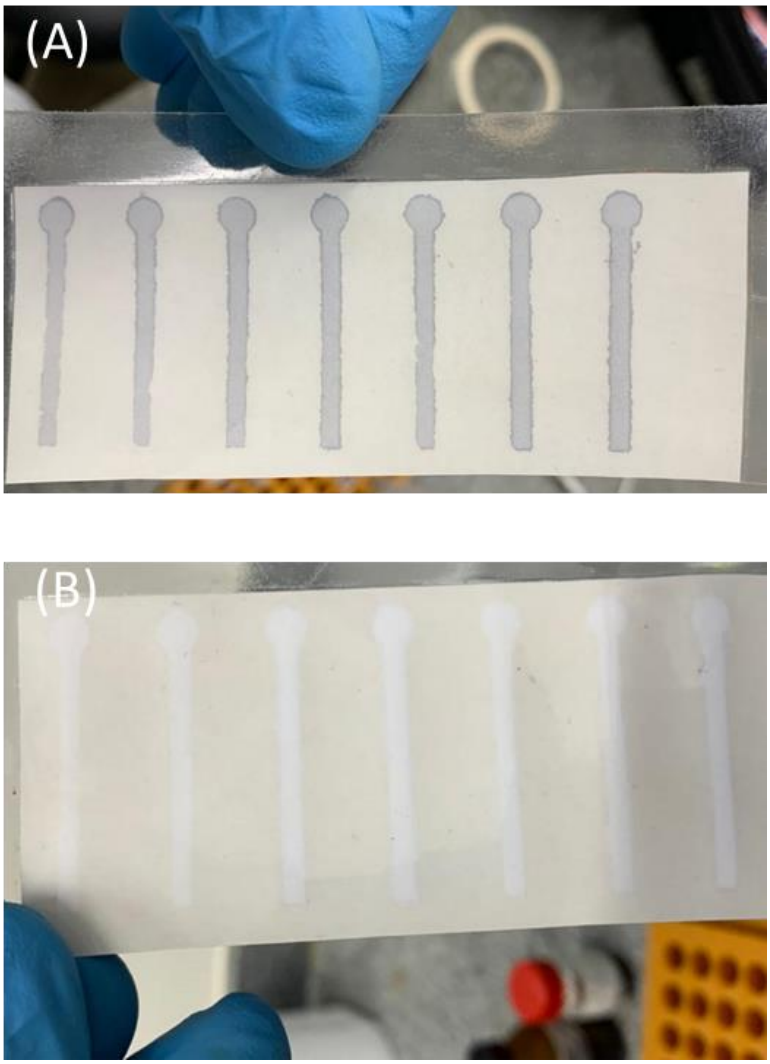

Figure S7. Effect of oxidation on office distance-based µPAD. In **(A)** microchannels with excess periodate on the surface and **(B)** microchannels before washing step with distilled water.

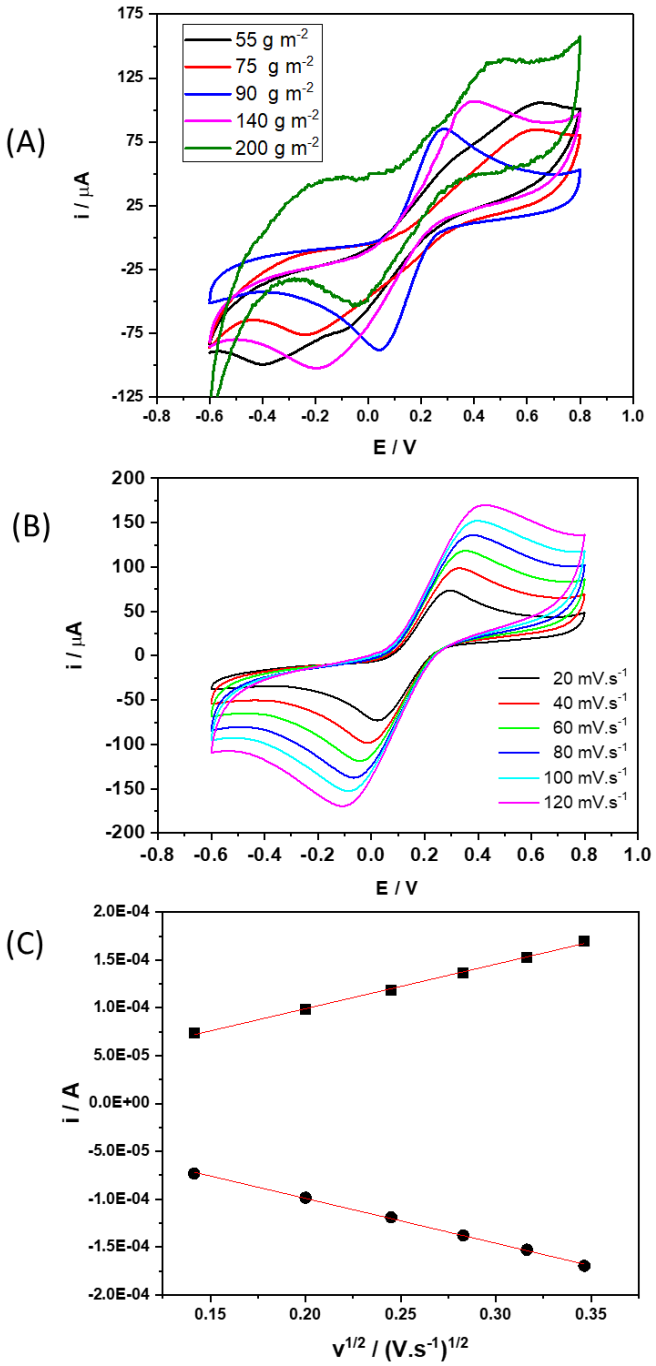

Figure S8. (A) Electrochemical profile of the ePADs in different grammages using CV at 50 mV s^{-1}; **(B)** S1 Study of scan rate (from 20 to 120 mV s^{-1}) of the electrodes in 0.1 mol L^{-1} KCl solution in presence of redox probe $[Fe(CN)6]^{3-/4-}$ (5.0 mmol L^{-1}) and; **(C)** Linear relation between Ip versus square root of scan rate. (R^2= 0.998), Y = $-5.42.10^{-6} – 4.69.10^{-4}$x ; R^2 = 0.997, Y = $6.08.10^{-6} + 4.65.10^{-4}$x

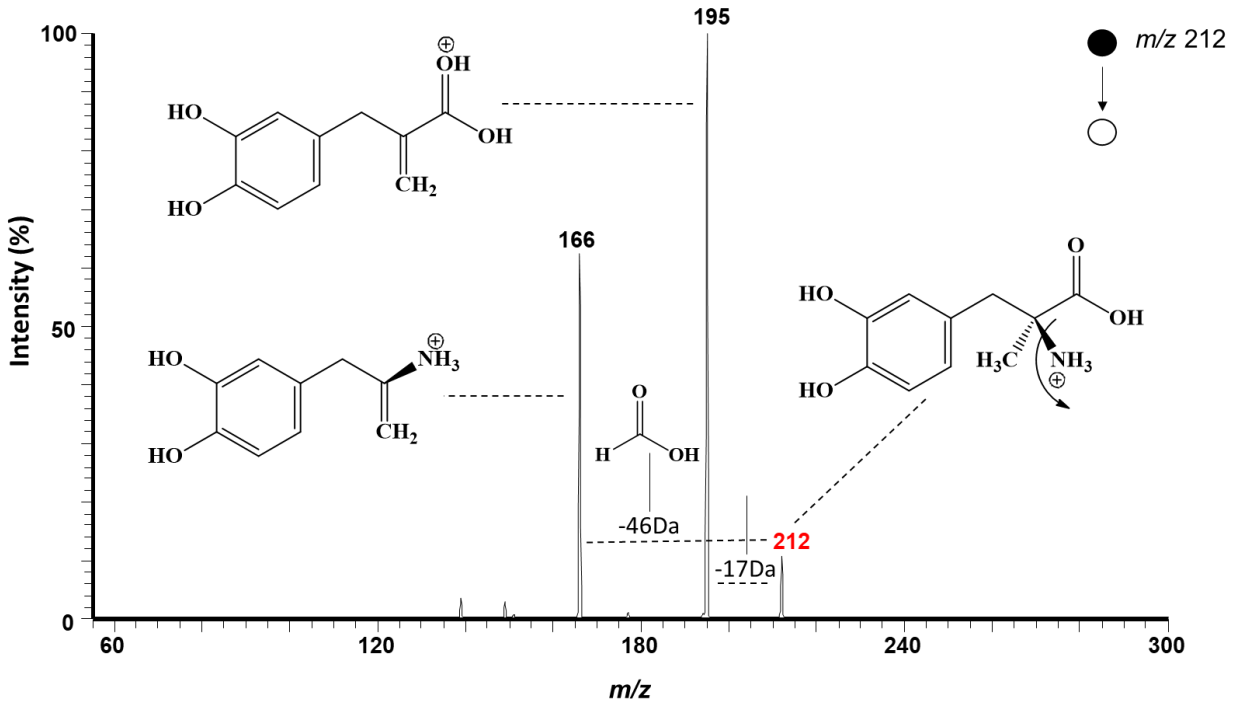

Figure S9. Fragmentation of target molecule by MS/MS

References

1 S. A. Nogueira, L. R. Sousa, N. K. L. Silva, P. H. F. Rodrigues and W. K. T. Coltro, *Micromachines*, 2017, **8**, 1–10.

2 L. R. Sousa, L. C. Duarte and W. K. T. Coltro, *Sensors Actuators, B Chem.*, 2020, **312**, 128018.

3 F. Pourkarim, E. Rahimpour, M. Khoubnasabjafari, V. Jouyban-Gharamaleki, A. Gharakhani and A. Jouyban, *Chem. Pap.*, 2021, **75**, 2901–2906.

4 L. Y. Shiroma, M. Santhiago, A. L. Gobbi and L. T. Kubota, *Anal. Chim. Acta*, 2012, **725**, 44–50.

5 S. H. Lee, J. H. Lee, V. K. Tran, E. Ko, C. H. Park, W. S. Chung and G. H. Seong, *Sensors Actuators, B Chem.*, 2016, **232**, 514–522.

6 I. V. S. Arantes and T. R. L. C. Paixão, *Talanta*, , DOI:10.1016/j.talanta.2021.123201.

7 P. Rattanarat, W. Dungchai, D. Cate, J. Volckens, O. Chailapakul and C. S. Henry, *Anal. Chem.*, 2014, **86**, 3555–3562.

8 H. A. Silva-Neto, T. M. G. Cardoso, C. J. McMahon, L. F. Sgobbi, C. S. Henry and W. K. T. Coltro, *Analyst*, 2021, **146**, 3463–3473.

9 J. C. Hofstetter, J. B. Wydallis, G. Neymark, T. H. Reilly, J. Harrington and C. S. Henry, *Analyst*, 2018, **143**, 3085–3090.

10 T. L. Mako, A. M. Levenson and M. Levine, *ACS Sensors*, 2020, **5**, 1207–1215.

11 E. Trofimchuk, Y. Hu, A. Nilghaz, M. Z. Hua, S. Sun and X. Lu, *Food Chem.*, , DOI:10.1016/j.foodchem.2020.126396.

12 F. T. S. M. Ferreira, R. B. R. Mesquita and A. O. S. S. Rangel, *Talanta*, 2020, **219**, 121183.

13 A. Charbaji, H. Heidari-Bafroui, C. Anagnostopoulos and M. Faghri, *Sensors (Switzerland)*, 2021, **21**, 1–15.

14 Y. Chen, X. Guo, W. Liu and L. Zhang, *Microchim. Acta*, , DOI:10.1007/s00604-019-3232-0.

15 F. Farschi, A. Saadati and M. Hasanzadeh, *Heliyon*, 2020, **6**, e04327.

16 F. Farshchi, A. Saadati, H. Kholafazad kordasht and M. Hasanzadeh, *ImmunoAnalysis*, 2021, **1**, 6–6.